



# Anchoring luminol based on $\text{Ti}_3\text{C}_2$ -mediated in situ formation of Au NPs for construction of an efficient probe for miRNA electrogenerated chemiluminescence detection

Tingting Zhuang<sup>1</sup> · Huixin Zhang<sup>1</sup> · Lun Wang<sup>1</sup> · Linhan Yu<sup>1</sup> · Zonghua Wang<sup>1</sup>

Received: 30 July 2021 / Revised: 29 August 2021 / Accepted: 3 September 2021 / Published online: 28 September 2021  
© Springer-Verlag GmbH Germany, part of Springer Nature 2021

## Abstract

An efficient electrogenerated chemiluminescence (ECL) nanoprobe (luminol-Au NPs- $\text{Ti}_3\text{C}_2$ ) was constructed based on  $\text{Ti}_3\text{C}_2\text{Tx}$  MXene ( $\text{Ti}_3\text{C}_2$ )-mediated in situ formation of Au NPs and anchoring luminol to fabricate a sensitive ECL biosensor for miRNA-155 detection. Herein,  $\text{Ti}_3\text{C}_2$  with rich Ti vacancy defects was used as reducing agent, and Au NPs were generated in situ and anchored on the  $\text{Ti}_3\text{C}_2$  (Au NPs- $\text{Ti}_3\text{C}_2$ ). Moreover, the Au NPs- $\text{Ti}_3\text{C}_2$  composites were used as a carrier and provided a large number of sites for the efficient linking of luminol through Au–N bonds to form stable luminol-Au NPs- $\text{Ti}_3\text{C}_2$ . The immobilization of ECL emitters is a versatile strategy which not only shortens the electron transmission distance between luminol and electrode, but also provides naked catalytic predominated (111) facets of Au NPs with high electrocatalytic activity, significantly improving the ECL signal of luminol. Furthermore, a catalytic hairpin assembly (CHA) reaction was used, resulting in further amplification of the signal. As a result, the as-prepared ECL biosensor exhibited a linear range from 0.3 fM to 1 nM with a detection limit of 0.15 fM, and demonstrated high reliability of miRNA-155 detection even in human serum samples. The construction of a multifunctional ECL probe with excellent ECL emission opens a new chapter for the application of  $\text{Ti}_3\text{C}_2$  in the field of bioanalysis.

**Keywords**  $\text{Ti}_2\text{C}_3\text{Tx}$  MXene · Ti vacancy defects · Luminol anchoring · Electrogenerated chemiluminescence · Probe · Signal amplification

## Introduction

Electrogenerated chemiluminescence (ECL) is light emission from a redox reaction of electrogenerated reactants. Therefore, it provides not only controllability of electrochemistry and high sensitivity of chemiluminescence, but also the advantages of all black background caused by electrical stimulation, no light bleaching and stable luminescence. It has been extensively adopted as suitable for biological systems with complex

components and extremely low concentration [1–3]. ECL biosensing plays a pivotal role in the biochemical analytical field. Enhancing biosensing interface performance and improving ECL efficiency are core scientific issues.

In recent years, immobilization of ECL emitters has been found to be an effective strategy to shorten the electron transfer distance between the luminophores and electrode surface and reduce the energy loss, thus improving ECL efficiency [4–8]. Luminol, as a classical important ECL luminescent material, has the inherent advantages of non-toxicity, low oxidation potential and high luminescent quantum yield [9–13]. However, it is difficult to immobilize luminol into the biosensing surface, owing to its lack of an active group [14–19]. For the traditional luminol system, high-quality active carriers are usually required to achieve immobilization of luminol. For example, luminol was used as an ECL luminescent material and reductant to form Pt nanoparticles on the surface of graphene sheets (GS) (Lu-Pt@GS) which functioned as an ECL sensing platform for highly sensitive detection of prostate-specific antigen (PSA) [20]. Luminol-functionalized

---

Tingting Zhuang and Huixin Zhang contributed equally to this work.

✉ Zonghua Wang  
wangzonghua@qdu.edu.cn

<sup>1</sup> College of Chemistry and Chemical Engineering, College of Materials Science and Engineering, Shandong Sino-Japanese Centre for Collaborative Research of Carbon Nanomaterials, Instrumental Analysis Centre of Qingdao University, Institute of Biomedical Engineering, Qingdao University, Qingdao 266071, Shandong, China

Ag NPs (luminol-Ag NPs) composite was adsorbed on Co/Ni-based metal-organic framework (MOF) nanosheets by electrostatic interaction to form luminol-Ag NPs@Co/Ni-MOF as an ECL platform for detection of alpha fetoprotein (AFP) [21]. Despite years of efforts, it is important to further improve the immobilization and enhance the ECL efficiency of luminol.

Two-dimensional (2D) transition metal carbides, nitrides or carbonitrides (MXenes) are a young family, and titanium carbide ( $\text{Ti}_3\text{C}_2\text{Tx}$ , Tx:  $-\text{OH}$ ,  $-\text{F}$  and other functional groups) is one of them, which was synthesized for the first time in 2011 [22]. It not only has the general advantages of traditional two-dimensional nanomaterials, but also has special surface structural properties, which make it popular for use in catalysis, sensing and other fields [23–29]. For example, in the field of catalysis, using the rich Ti vacancy defects and high reduction ability of  $\text{Ti}_3\text{C}_2\text{Tx}$  nanosheets, Pt atoms occupy the Ti defect sites through Pt–C bonds and are anchored on ultrathin  $\text{Ti}_3\text{C}_2$  nanosheets to prepare single-atom catalyst (SAC)-Pt/ $\text{Ti}_3\text{C}_2\text{Tx}$ , which realizes the effective functionalization of carbon dioxide ( $\text{CO}_2$ ) [30]. In the field of electrochemical sensing,  $\text{Ti}_3\text{C}_2\text{Tx}/\text{Ag}$  composites have been synthesized via the strong reducing property of  $\text{Ti}_3\text{C}_2\text{Tx}$ . It promotes electron transfer at the sensing interface because of the unique electrocatalytic properties of  $\text{Ti}_3\text{C}_2\text{Tx}$  nanosheets and Ag NPs, and an acetylcholinesterase biosensor has been constructed [31]. In the field of energy storage, based on the advantages of  $\text{Ti}_3\text{C}_2\text{Tx}$ , such as high conductivity and large specific surface area, it can be used as a new type of high-capacity battery material [32]. At the same time, the terminated groups such as  $-\text{F}$  and  $-\text{OH}$  groups make  $\text{Ti}_3\text{C}_2$  negatively charged, with good hydrophilicity [33–35]. Although  $\text{Ti}_3\text{C}_2\text{Tx}$  was first used in an ECL biosensor in 2018, research on its use in ECL biosensors is still in a period of vigorous development.

In our strategy, luminol-Au NPs- $\text{Ti}_3\text{C}_2$  nanoprobe were synthesized in situ based on the unique abundant Ti vacancy defects and Au–N bonds (Scheme 1a). Au NPs were generated in situ and anchored on  $\text{Ti}_3\text{C}_2$  to form stable Au NPs- $\text{Ti}_3\text{C}_2$  composites. In addition, the luminol could be effectively immobilized via Au–N bonds in the Au NPs- $\text{Ti}_3\text{C}_2$  composites. The multifunctional and efficient luminol-Au NPs- $\text{Ti}_3\text{C}_2$  nanoprobe could shorten the electron transmission distance between the luminol and electrode interface and accelerate the electron transmission. Meanwhile, it provides naked catalytic predominated (111) facets of Au NPs with high electrocatalytic activity, which can significantly improve the ECL signal of luminol. This way of in situ anchoring provides a new strategy for the construction of nanoprobe with excellent performance. It is expected that the generation and amplification of an ECL signal can be realized in a very simple and effective way.

The design for the ECL biosensor is shown in Scheme 1b. SA/PAM was modified on the electrode surface, which provided more binding sites for sDNA. After that, the catalytic hairpin assembly (CHA) reaction, a thermostatic, enzyme-

free, low-cost amplification and simulated target DNA with negligible background at high-speed strategy [36, 37], can realize the cycle of miRNA-155, and the luminol-Au NPs- $\text{Ti}_3\text{C}_2$  nanoprobe can be efficiently modified on the electrode by complementary pairing of sDNA and H2, which promote the amplification of the ECL signal of luminol. The as-designed ECL biosensor has good specificity and remarkable stability, showing a lower detection limit, and the linear range was over three orders of magnitude. It was also applicable for miRNA-155 detection in human serum samples. This will provide a new perspective for the design of signal amplification strategy based on the combination of nucleic acid and  $\text{Ti}_3\text{C}_2$ .

## Experimental section

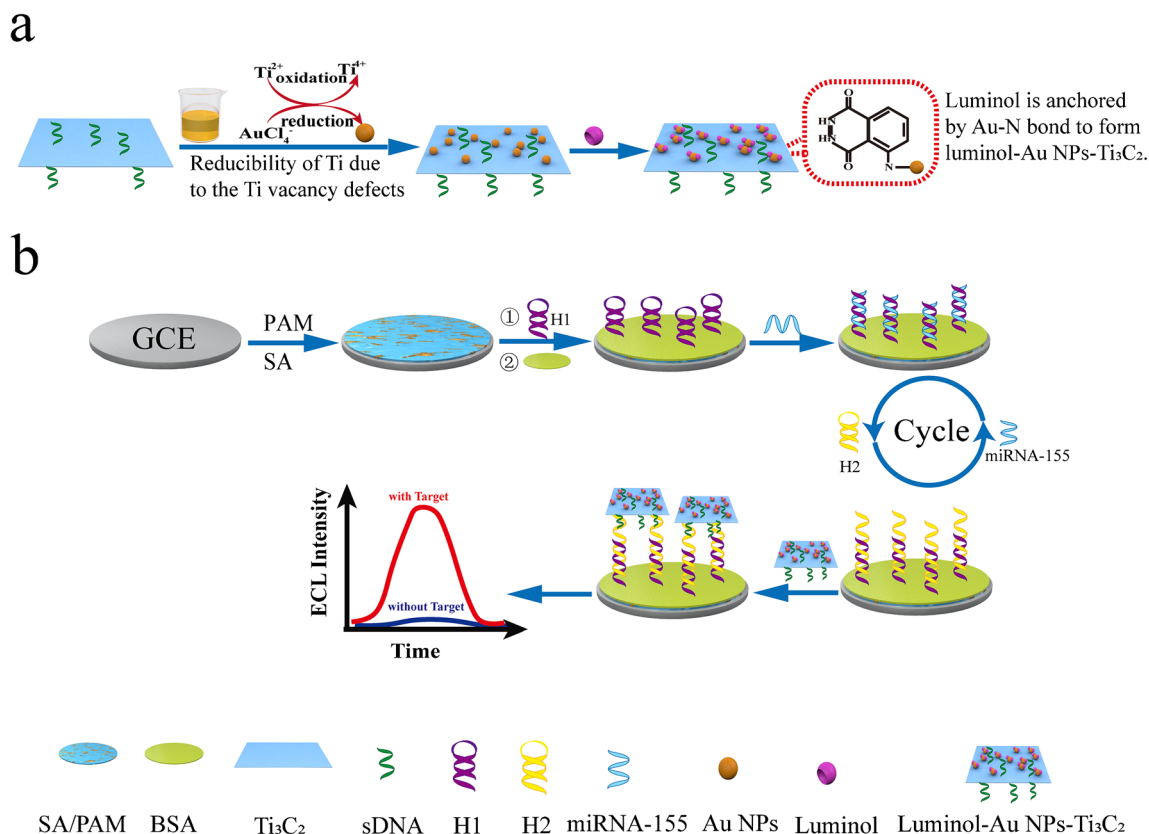
The subsection describing the reagents and materials, instruments and the preparation of  $\text{Ti}_3\text{C}_2$  is presented in the Supporting Information.

### Formation of luminol-Au NPs- $\text{Ti}_3\text{C}_2$

The  $\text{Ti}_3\text{C}_2$ -glycine hybrid was synthesized as described in previous work [38]. Ten milliliters of  $\text{Ti}_3\text{C}_2$  solution ( $0.075 \text{ mg mL}^{-1}$ ) was added dropwise to glycine solution ( $20 \text{ mL}$ ,  $0.25 \text{ mg mL}^{-1}$ ) and stirred for 24 h. Then, the suspension was centrifuged to separate the solid, obtaining  $\text{Ti}_3\text{C}_2$ -glycine solution. After that,  $60 \mu\text{L}$  sDNA solution ( $6 \mu\text{M}$ ) was activated using EDC ( $400 \text{ mM}$ ) and NHS ( $100 \text{ mM}$ ) at  $37 \text{ }^\circ\text{C}$  for 1 h. Then,  $300 \mu\text{L}$   $\text{Ti}_3\text{C}_2$ -glycine solution was injected into the sDNA mixed solution. After stirring for 1 h, the precipitate was retained through centrifugation and dispersed in deionized water (DI) to obtain sDNA- $\text{Ti}_3\text{C}_2$ -glycine (sDNA- $\text{Ti}_3\text{C}_2$ ).  $\text{HAuCl}_4$  solution ( $125 \mu\text{L}$ ,  $2 \text{ mg mL}^{-1}$ ) was added into sDNA- $\text{Ti}_3\text{C}_2$  solution and stirred to obtain sDNA-Au NPs- $\text{Ti}_3\text{C}_2$  (Au NPs- $\text{Ti}_3\text{C}_2$ ). Next,  $300 \mu\text{L}$  luminol solution ( $0.75 \text{ mg mL}^{-1}$ ) was injected in the AuNPs- $\text{Ti}_3\text{C}_2$  solution ( $300 \mu\text{L}$ ) and stirred. Finally, the luminol-Au NPs- $\text{Ti}_3\text{C}_2$  was obtained for the subsequent use.

### Construction of the proposed ECL biosensor

The construction process of the biosensor is shown in Scheme 1 b. The glassy carbon electrode (GCE) was polished with  $0.3$  and  $0.05 \mu\text{m}$   $\alpha\text{-Al}_2\text{O}_3$  powder and ultrasonically cleaned in ethanol and DI water, and was then immediately used for the next step. Firstly,  $6 \mu\text{L}$  PAM solution ( $0.1 \text{ mg mL}^{-1}$ ) was added on the surface of GCE and dried under air to obtain PAM/GCE. At the same time,  $500 \mu\text{L}$  SA solution ( $10 \text{ mg mL}^{-1}$ ) was added to  $2 \text{ mL}$  MES buffer. After stirring,  $250 \mu\text{L}$



**Scheme 1** (a) Strategy of stable luminol-Au NPs-Ti<sub>3</sub>C<sub>2</sub>. (b) Construction of the proposed ECL biosensor

EDC (200 mM) and 250  $\mu$ L NHS (600 mM) were added to the mixed solution at 37  $^{\circ}$ C for 1 h to activate the carboxyl group of SA. Then, the PAM/GCE was immersed in the mixed solution at 37  $^{\circ}$ C for 1 h to obtain SA/PAM/GCE. Subsequently, 10  $\mu$ L H1 solution (2  $\mu$ M) was added dropwise to SA/PAM/GCE and incubated at room temperature for 2 h to obtain H1/SA/PAM/GCE. After that, 5  $\mu$ L 1% BSA solution was added dropwise to the H1/SA/PAM/GCE and incubated at 37  $^{\circ}$ C for 1 h to block nonspecific binding sites and obtain BSA/H1/SA/PAM/GCE. Next, the mixed solution containing H2 (6  $\mu$ L, 4  $\mu$ M) and miRNA-155 (6  $\mu$ L) solution was dropped on the surface of the BSA/H1/SA/PAM/GCE and incubated at room temperature for 2 h to initiate the CHA reaction and obtain the H2 + H1/BSA/SA/PAM/GCE. Finally, 10  $\mu$ L luminol-Au NPs-Ti<sub>3</sub>C<sub>2</sub> nanoprobe was added on the surface of the GCE and incubated for 2 h at room temperature to obtain the luminol-Au NPs-Ti<sub>3</sub>C<sub>2</sub>/H2 + H1/BSA/SA/PAM/GCE.

## Results and discussion

### ECL measurement of detection

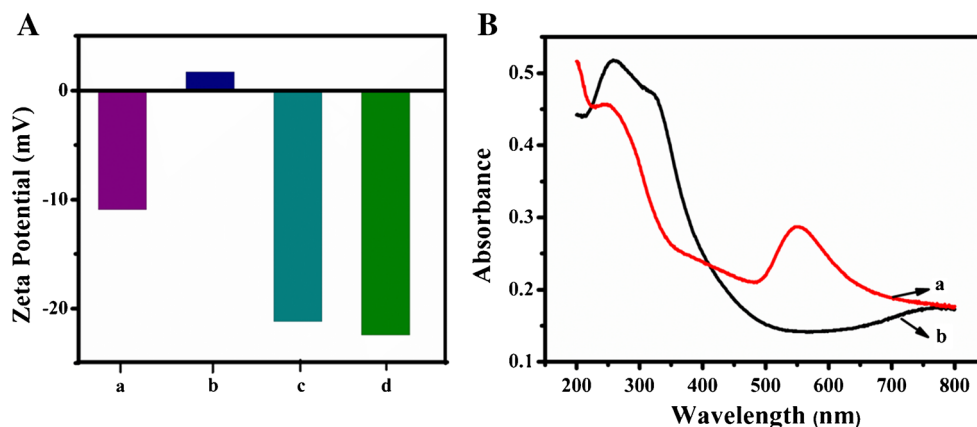
To detect miRNA-155, the modified GCE was reacted in 15 mL of phosphate-buffered saline (PBS) (0.1 M, pH 7.4)

containing 10 mM H<sub>2</sub>O<sub>2</sub>. In this study, a three-electrode system was used, the working electrode was the GCE, the reference electrode was Ag/AgCl (saturated KCl), and the auxiliary electrode was a platinum wire. The scanning potential was set from 0 to 0.6 V, and the scanning speed was 0.1 V/s. The high voltage of the photomultiplier tube was 850 V.

### Characterization of Ti<sub>3</sub>C<sub>2</sub>, Au NPs-Ti<sub>3</sub>C<sub>2</sub> and luminol-Au NPs-Ti<sub>3</sub>C<sub>2</sub>

To verify the successful synthesis of Ti<sub>3</sub>C<sub>2</sub> and Au NPs-Ti<sub>3</sub>C<sub>2</sub>, transmission electron microscopy (TEM), X-ray diffraction (XRD), X-ray photoelectron spectroscopy (XPS), electrophoretic light scattering (ELS) and UV-vis analyses were performed. The ELS data are shown in Fig. 1A: Ti<sub>3</sub>C<sub>2</sub> nanosheets exhibit negative potential (a), Ti<sub>3</sub>C<sub>2</sub> modified with glycine shows positive potential (b), and the Ti<sub>3</sub>C<sub>2</sub>-sDNA composites show highly negative zeta potential due to the negative charge of the nucleic acid sequence (c). The above results indicate that sDNA was linked with Ti<sub>3</sub>C<sub>2</sub> successfully. Au NPs-Ti<sub>3</sub>C<sub>2</sub>-sDNA (Au NPs-Ti<sub>3</sub>C<sub>2</sub>) was synthesized by in situ formation of Au NPs in the presence of negative charge (d). Meanwhile, as Fig. 1B shows, compared with the UV-vis absorption curve of Ti<sub>3</sub>C<sub>2</sub> (b), the spectrum of Au NPs-Ti<sub>3</sub>C<sub>2</sub> shows characteristic peaks of Au NPs at about 550 nm and the characteristic peaks of Ti<sub>3</sub>C<sub>2</sub> at about

**Fig. 1** (A) The ELS data of  $\text{Ti}_3\text{C}_2$  (a),  $\text{Ti}_3\text{C}_2$ -glycine (b),  $\text{Ti}_3\text{C}_2$ -sDNA (c), Au NPs- $\text{Ti}_3\text{C}_2$ -sDNA (d). (B) The UV-vis analysis of Au NPs- $\text{Ti}_3\text{C}_2$  (a) and  $\text{Ti}_3\text{C}_2$  (b)



280 nm (a). Furthermore, XRD analysis supports the conclusion as well. Fig. S1A shows the XRD patterns of  $\text{Ti}_3\text{AlC}_2$  (a) and  $\text{Ti}_3\text{C}_2$  (b). Compared with the XRD pattern of  $\text{Ti}_3\text{AlC}_2$  (Fig. S1A curve a), the main peak (104) disappears, and the peak (002) shifts to the left in the case of  $\text{Ti}_3\text{C}_2$  (Fig. S1A curve b), which means that  $\text{Ti}_3\text{C}_2$  nanosheets were successfully prepared. In addition, the specific diffraction peaks of Au, such as (111), (200), (220) and (311) planes, are also shown in Fig. S1A curve c. The result indicates the presence of Au NPs- $\text{Ti}_3\text{C}_2$ . As shown in TEM images (Fig. S1B), the monodisperse morphology of  $\text{Ti}_3\text{C}_2$  with an average diameter of approximately 200 nm is observed, which confirms the successful exfoliation of  $\text{Ti}_3\text{C}_2$  nanosheets. In Fig. S1C, it can be clearly seen that Au NPs were anchored on the  $\text{Ti}_3\text{C}_2$  nanosheets. The XPS patterns of  $\text{Ti}_3\text{C}_2$  and Au NPs- $\text{Ti}_3\text{C}_2$  can be clearly observed (Fig. S2A). Compared with the XPS spectrum of  $\text{Ti}_3\text{C}_2$ , Au appears in the Au NPs- $\text{Ti}_3\text{C}_2$ . In Fig. S2B, the peaks at 454–457.5 eV indicate the possible existence of low-priced Ti species, such as Ti (II) at 455 eV, Ti-C at 456 eV, and Ti-O at 461.3 eV. In addition, it is shown in Fig. S2C that the synthesis of Au NPs results in the transfer of Ti (II) to Ti (IV). Figure S2D shows peaks at 83.7 and 87.3 eV, and the binding energy gap is 3.6 eV, which are obvious Au 4f peaks. The above results indicate the successful preparation of Au NPs- $\text{Ti}_3\text{C}_2$ .

In order to verify the successful synthesis of luminol-Au NPs- $\text{Ti}_3\text{C}_2$ , the results were confirmed by energy-dispersive X-ray spectroscopy (EDS) elemental mapping and Fourier transform infrared (FT-IR) analysis. Figure 2A shows the elemental mapping diagram (EDS) of the luminol-Au NPs- $\text{Ti}_3\text{C}_2$ . Ti, Au and N are present, in which Ti comes from  $\text{Ti}_3\text{C}_2$ , Au comes from in situ generated Au NPs, and N is mainly distributed on the surface of Au NPs, indicating that it mainly comes from luminol. As shown in Fig. 2B, the ultraviolet absorption spectrum of luminol has three absorption bands lying at 221 nm, 300 nm and 350 nm which correspond to the carbonyl group, N–N and  $-\text{NH}_2$ , respectively, in the structure of luminol (curve b). There is a peak at 550 nm in addition to characteristic peak corresponding to luminol

which is the characteristic peaks of Au NPs (curve a). The result indicates the formation of luminol-Au NPs- $\text{Ti}_3\text{C}_2$ . As Fig. S3 shows, compared with the FT-IR spectrum of  $\text{Ti}_3\text{C}_2$  (a), characteristic peaks at  $\sim 1348\text{ cm}^{-1}$  and  $\sim 1489\text{ cm}^{-1}$  appear in the infrared spectrum of the luminol-Au NPs- $\text{Ti}_3\text{C}_2$  (b), which are mainly attributed to the stretching vibration of the nitrogen impurity naphthalene ring and the C=C vibration in the luminol structure. The FT-IR spectrum further intuitively proves the successful synthesis of luminol-Au NPs- $\text{Ti}_3\text{C}_2$ . Figure 2C shows the ECL spectra of luminol and luminol-Au NPs- $\text{Ti}_3\text{C}_2$ ; the ECL emission peaks of both are about 445 nm. It comes from luminol which was oxidized to 3-aminophthalate and finally emits light, which means that the structure of luminol remains unchanged after bonding with Au NPs- $\text{Ti}_3\text{C}_2$ . In addition, the stability of luminol-Au NPs- $\text{Ti}_3\text{C}_2$  was evaluated. As Fig. S4 shows, luminol-Au NPs- $\text{Ti}_3\text{C}_2$  shows excellent chemical stability in the ECL experiment, thus achieving stable ECL intensity under scanning for 10 consecutive cycles. The above results indicate that stable and effective luminol-Au NPs- $\text{Ti}_3\text{C}_2$  was successfully synthesized.

### Polyacrylamide gel electrophoresis (PAGE) analysis of the ECL biosensor

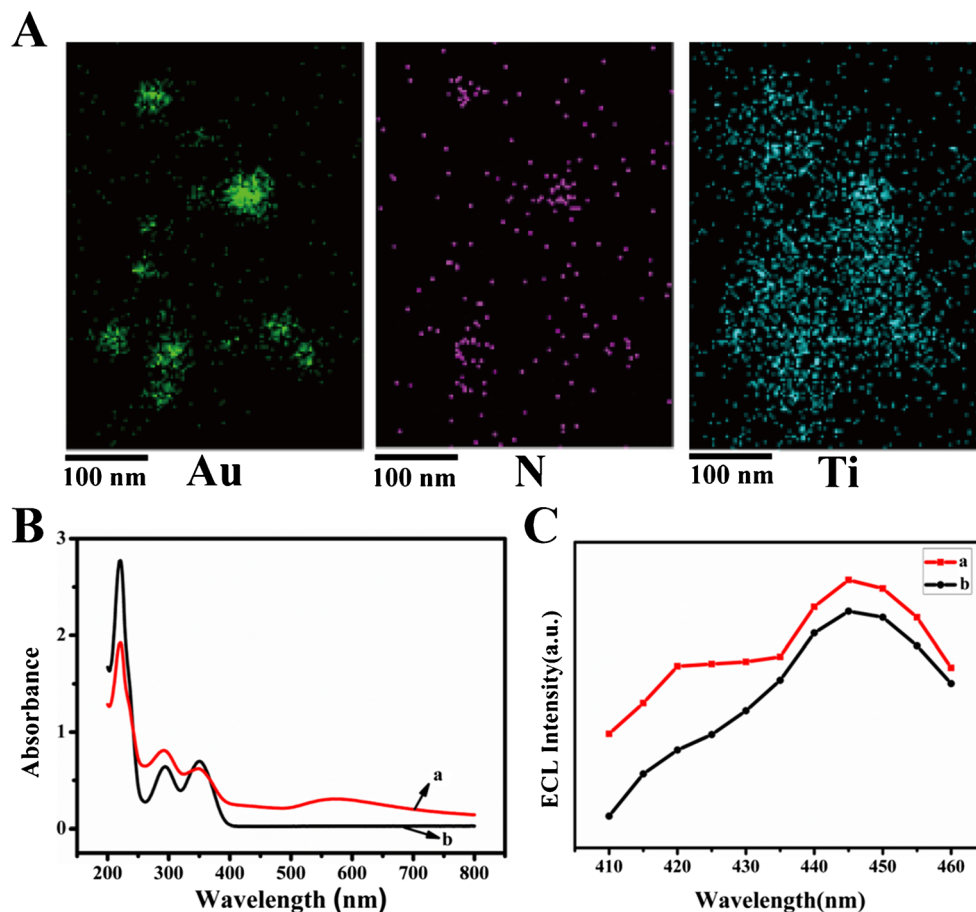
To verify the feasibility of this strategy and the interaction between experimental DNA and miRNA sequences, the 8% PAGE analysis was performed, as presented in Fig. S5. The result shows that for the analysis of the CHA reaction process, the DNA and miRNA reactions at every step are in accord with the proposed strategy.

### Electrochemical characterization of the assembly processes of the biosensor

The step-by-step assembly procedure of the biosensor was confirmed by cyclic voltammetry (CV) and electrochemical impedance spectroscopy (EIS) in a solution of 5 mM  $[\text{Fe}(\text{CN})_6]^{3-/4-}$  containing 0.1 M KCl. The CV curves are



**Fig. 2** (A) The elemental mapping of luminol-Au NPs-Ti<sub>3</sub>C<sub>2</sub> composites. (B) The UV-vis analysis of luminol-Au NPs-Ti<sub>3</sub>C<sub>2</sub>(a) and luminol (b). (C) ECL spectra of luminol-Au NPs-Ti<sub>3</sub>C<sub>2</sub>(a) and luminol (b) in the solution with H<sub>2</sub>O<sub>2</sub>



shown in Fig. S6A, in which the bare GCE exhibits a pair of significant redox peaks of  $[\text{Fe}(\text{CN})_6]^{3-/4-}$ . The peak current of  $[\text{Fe}(\text{CN})_6]^{3-/4-}$  at the SA/PAM/GCE decreases owing to the electrical resistance effect of SA/PAM. When H1 and H2 were gradually modified on the surface of the GCE, the peak current was further decreased due to the increase in nonconductive biomacromolecules. After incubation with the luminol-Au NPs-Ti<sub>3</sub>C<sub>2</sub> nanoprobe, the peak current was slightly lower. Figure S6B shows the assembly steps of the electrode characterized by EIS. Firstly, a small semicircle of bare GCE is observed. With step-by-step assembly, the diameter of the curved semicircle increases successively, indicating that the electron transfer resistance gradually increases. These data indicate the successful construction of the ECL biosensor.

### The control experiment of the ECL biosensor

To confirm the efficiency of the luminol-Au NPs-Ti<sub>3</sub>C<sub>2</sub>/H2 + H1/SA/PAM/GCE, control experiments were performed. One of the control experiments was designed without sDNA at the Ti<sub>3</sub>C<sub>2</sub>, and the resulting luminol-Au NPs-Ti<sub>3</sub>C<sub>2</sub> could not be trapped on the electrode (Fig. 3 a). The second experiment was designed without HAuCl<sub>4</sub> in Scheme 1a for testing the

catalytic ability of the Au NPs (Fig. 3 b). Moreover, without the formation of Au NPs, luminol could not be effectively immobilized by Au-N bonds. As shown in Fig. 3, it can clearly be seen that the ECL intensity (c) is the highest as compared with (a) and (b). The ECL-potential curves of (a), (b) and (c) in Fig. S7A have the same trend as in Fig. 3. Moreover, the ECL-potential curves of (a) and (b) display onset potential at approximately 0.46 V, and the ECL-potential curve of (c)

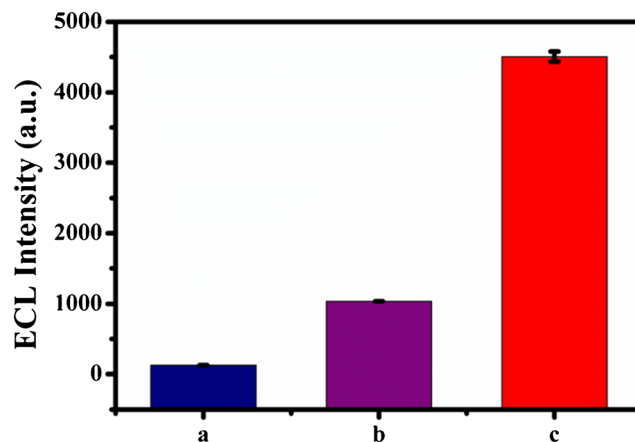


**Fig. 3** Comparison of ECL intensity of the biosensor: (a) without sDNA at the Ti<sub>3</sub>C<sub>2</sub>, (b) without the formation of Au NPs, (c) designed biosensor. The concentration of miRNA-155 is 100 fM

**Table 1** Comparison of proposed assay with reported works for determination of miRNA

Analytical method	Linear range	Detection Limit	Ref.
Fluorescence	1.02 nM–144 nM	0.18 nM	[39]
Electrochemistry	10.0 fM–1.00 nM	1.64 fM	[40]
SPR	50.0 pM–5.00 nM	45.0 pM	[41]
ECL	1.00 pM–10.0 $\mu$ M	0.67 pM	[42]
ECL	10.0 fM–100 nM	5.70 fM	[43]
ECL	0.3 fM–1.0 nM	0.15 fM	This work

displays an onset potential at approximately 0.32 V due to the conductivity and catalytic properties of Au NPs-Ti<sub>3</sub>C<sub>2</sub>. Meanwhile, CV curves in Fig. S7B show that the current of (c) is significantly higher compared with (a) and (b), which shows that the generated gold nanoparticles improve the charge transfer and increase the current. The strong ECL signal of luminol-Au NPs-Ti<sub>3</sub>C<sub>2</sub>/H<sub>2</sub> + H1/BSA/SA/PAM/GCE is mainly due to the in-situ formation and anchoring of Au NPs to form Au NPs-Ti<sub>3</sub>C<sub>2</sub> and then immobilization of a large amount of luminol through Au-N bonds, which can shorten the electron transmission and reduce energy loss to improve ECL efficiency. In addition, the good conductivity and electrocatalytic activity of Au NPs-Ti<sub>3</sub>C<sub>2</sub> can promote the reduction of H<sub>2</sub>O<sub>2</sub>, and resulting reactive oxygen species such as O<sub>2</sub><sup>•</sup> can further oxidize luminol and improve the ECL intensity.

### ECL detection of miRNA-155

shows the assembly steps of the eIn order to study the performance of the prepared biosensor, we measured the ECL response of different concentrations of miRNA-155 under the best experimental conditions (Fig. S8). It can be seen from

Fig. 4A that ECL intensity increases as the miRNA-155 concentration increases. Figure 4B shows that the ECL intensity of the biosensor has a good linear relationship range from 0.3 fM to 1.0 nM with the logarithm of miRNA-155 concentration. The linear equation is  $I = 7112.2 + 198.5 \lg C$  ( $I$  represents ECL intensity,  $C$  represents the concentration of miRNA-155). The limit of detection (LOD) was calculated to be 0.15 fM with a correlation coefficient of  $R^2 = 0.9923$ . As shown in Table 1, the performance comparison between the developed ECL biosensor and those reported previously reveals that the biosensor has higher sensitivity and wider linear range.

### Selectivity and stability of the proposed biosensor

In order to evaluate the practicability of the prepared ECL biosensor, its selectivity and stability were also studied. By exploring the ECL response of interfering substances, the specificity of the developed biosensor for miRNA-155 detection was proved. By using blank solution (miRNA-155, 0 pM), non-complementary DNA (nDNA, 1 pM), non-complementary RNA (nRNA, 1 pM), single-base difference RNA (sRNA, 1 pM) and perfect complementary sequence (miRNA-155, 100 fM) solution were used to evaluate its specificity. According to the measurement results of four parallel tests under the same experimental conditions, as shown in Fig. 5A, the developed biosensor has the best ECL response for miRNA-155, compared with the excess (10 times) interference from non-target analytes and the blank. This shows that the developed biosensor has good specificity, which is attributed to the sequence of miRNA-155 in this system that specifically recognizes H1. Stability is another important criterion for studying biosensor performance. The stability of the prepared biosensor was investigated by continuous

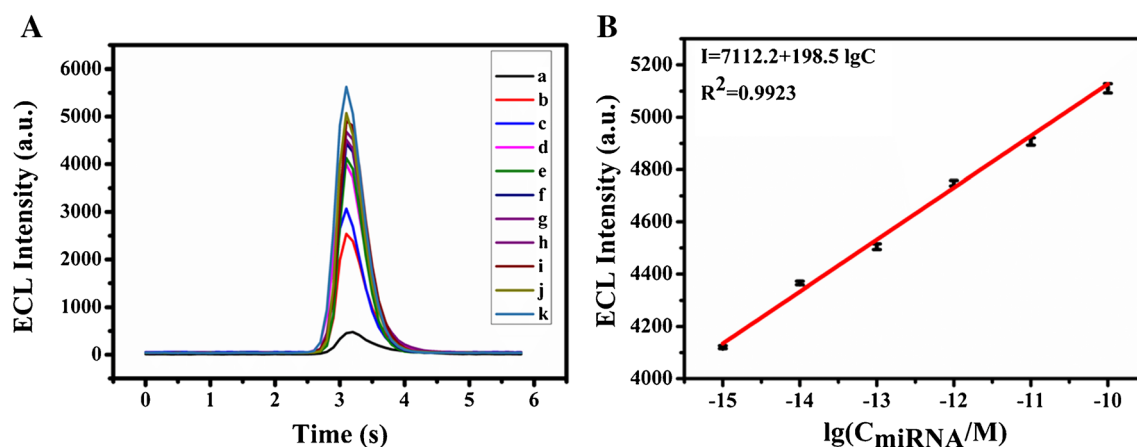


**Fig. 4** (A) ECL detection of miRNA-155 at different concentrations. (a) 0 fM, (b) 0.3 fM, (c) 0.5 fM, (d) 0.8 fM, (e) 1.0 fM, (f) 10 fM, (g) 100 fM, (h) 1.0 pM, (i) 10 pM, (j) 100 pM, (k) 1.0 nM in the detection solution.

**(B)** The linear relationship between the ECL intensity and the logarithm of concentration of miRNA-155

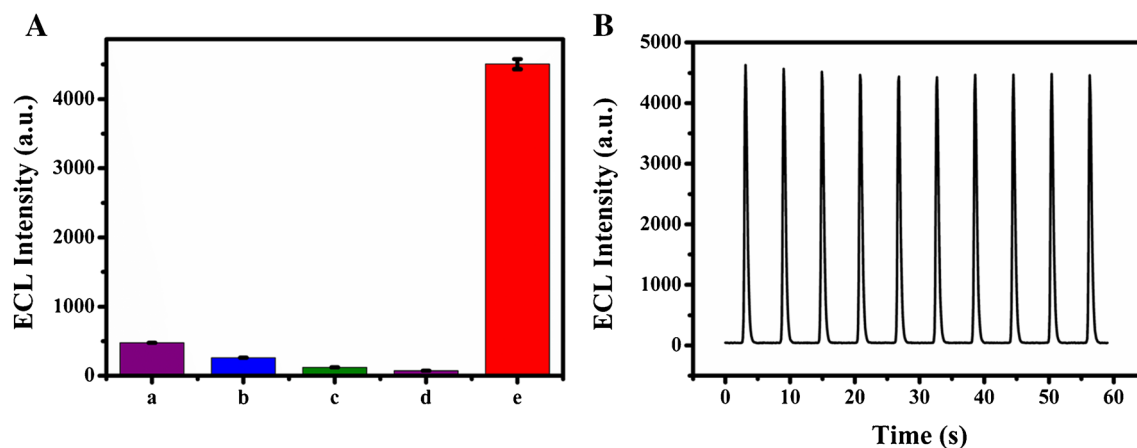


**Fig. 5** (A) The selectivity of the biosensor toward miRNA-155 detection. From a to e: blank, non-complementary DNA (nDNA, 1.0 pM), non-complementary miRNA (nrRNA, 1.0 pM), single-base difference

miRNA (srRNA, 1.0 pM), and miRNA-155 (100 fM) in the detection solution. (B) Stability of the ECL biosensor. The concentration of miRNA-155 is 100 fM

cyclic scanning for 10 cycles in the PBS solution (0.1 M, pH 7.4) containing 10 mM H<sub>2</sub>O<sub>2</sub> and recorded in Fig. 5B. The ECL intensities exhibited almost no fluctuation, which demonstrated that the ECL sensor possessed superior reproducibility.

### Application in human serum samples

In order to verify the practical applicability of the biosensor, a recovery experiment of miRNA-155 determination was carried out in human serum. Firstly, the serum was diluted 10 times. Then, different concentrations of miRNA-155 were injected into the serum. As shown in Table 2, the recovery was 95.50–107.15%, and the intra-assay relative standard deviation (RSD) was 4.12, 5.31, 7.32 and 7.94% at 1 fM, 10 fM, 100 fM and 1 pM of miRNA-155, respectively, which indicates that the biosensor is feasible for detecting miRNA-155 in actual samples.

### Conclusion

In summary, we developed a novel and sensitive ECL biosensor by using luminol-modified in situ formation of Au NP-decorated Ti<sub>3</sub>C<sub>2</sub> MXene hybrid (luminol-Au NPs-Ti<sub>3</sub>C<sub>2</sub>) as ECL nanoprobe and CHA reaction as signal amplification

for the detection of miRNA-155. Ti<sub>3</sub>C<sub>2</sub> was used as the reductive nanocarrier for the in situ generation and anchoring of Au NPs to form Au NPs-Ti<sub>3</sub>C<sub>2</sub>. Furthermore, the luminol-Au NPs-Ti<sub>3</sub>C<sub>2</sub> nanoprobe were directly formed through Au–N bonds. This simplifies the synthesis of luminol-Au NPs-Ti<sub>3</sub>C<sub>2</sub>, increases the immobilization of luminol, and shortens the electron transmission distance between the luminol and electrode interface. More importantly, Au NPs-Ti<sub>3</sub>C<sub>2</sub> with good conductivity and catalysis, combined with the CHA signal amplification strategy, can achieve dual amplification of the luminol ECL signal and improve the sensitivity of the biosensor for miRNA-155, with a detection limit of 0.15 fM. The proposed ECL biosensor can be effectively applied to detect miRNA-155 in complex serum samples with recovery of 95.50–107.15%. These results indicate that the ECL biosensor has potential practical value in clinical diagnosis.

**Supplementary Information** The online version contains supplementary material available at <https://doi.org/10.1007/s00216-021-03651-7>.

**Acknowledgements** This work was financially supported by the Taishan Scholar Program of Shandong Province (ts201511027) and the Natural Science Foundation of Shandong Province (ZR2020MB063), China.

**Author contributions** Tingting Zhuang: Data curation, Writing – original draft, Investigation, Drafted and revised the manuscript. Huixin Zhang: Methodology, Writing – review & editing, Investigation, Design. Lun Wang: Characterization, Writing – review & editing. Linhan Yu: Routine analysis. Zonghua Wang: Methodology, Writing – review & editing, Supervision, Funding acquisition. All authors discussed the results and contributed to the writing of this manuscript. All authors have given approval to the final version of the manuscript. Tingting Zhuang and Huixin Zhang contributed equally to this work.

**Declarations** The authors declare that there is no conflict of interest.

The human serum samples used in this work were obtained from the hospital (The Affiliated Hospital of Qingdao University, Qingdao, China), and the ethics committee of the hospital approved the study.

**Table 2** Determination of miRNA-155 in human serum samples

Sample	Added (M)	Found (M)	RSD (%)	Recovery (%)
1	$1.00 \times 10^{-15}$	$9.55 \times 10^{-16}$	4.12	95.50
2	$1.00 \times 10^{-14}$	$1.07 \times 10^{-14}$	5.31	107.15
3	$1.00 \times 10^{-13}$	$1.05 \times 10^{-14}$	7.32	104.71
4	$1.00 \times 10^{-12}$	$1.00 \times 10^{-12}$	7.94	100.00

## References

- Li L, Chen Y, Zhu JJ. Recent advances in electrochemiluminescence analysis. *Anal Chem.* 2017;89:358–71.
- Ma C, Cao Y, Gou X, Zhu JJ. Recent progress in electrochemiluminescence sensing and imaging. *Anal Chem.* 2020;92:431–54.
- Zhang S, Liu Y. Recent progress of novel electrochemiluminescence nanoprobes and their analytical applications. *Front Chem.* 2020;8:626243.
- Fan Z, Yao B, Ding Y, Zhao J, Xie M, Zhang K. Entropy-driven amplified electrochemiluminescence biosensor for RdRp gene of SARS-CoV-2 detection with self-assembled DNA tetrahedron scaffolds. *Biosens Bioelectron.* 2021;178:113015.
- Liu PF, Zhao KR, Liu ZJ, Wang L, Ye SY, Liang GX. Cas12a-based electrochemiluminescence biosensor for target amplification-free DNA detection. *Biosens Bioelectron.* 2021;176:112954.
- Nasrollahpour H, Mahdipour M, Isildak I, Rashidi MR, Naseri A, Khalilzadeh B. A highly sensitive electrochemiluminescence cytosensor for detection of SKBR-3 cells as metastatic breast cancer cell line: a constructive phase in early and precise diagnosis. *Biosens Bioelectron.* 2021;178:113023.
- Zhang K, Fan Z, Ya B, Ding Y, Zhao J, Xie M, Pan J. Exploring the tans-cleavage activity of CRISPR-Cas12a for the development of a Mxene based electrochemiluminescence biosensor for the detection of Siglec-5. *Biosens Bioelectron.* 2021;178:113019.
- Zhu L, Yu L, Ye J, Yan M, Peng Y, Huang J, Yang X. A ratiometric electrochemiluminescence strategy based on two-dimensional nanomaterial-nucleic acid interactions for biosensing and logic gates operation. *Biosens Bioelectron.* 2021;178:113022.
- Gan X, Han D, Wang J, Liu P, Li X, Zheng Q, Yan Y. A highly sensitive electrochemiluminescence immunosensor for h-FABP determination based on self-enhanced luminophore coupled with ultrathin 2D nickel metal-organic framework nanosheets. *Biosens Bioelectron.* 2021;171.
- Sornambigai M, Venkateswara Raju C, Senthil KS. Bimodal electrogenerated chemiluminescence of the luminol/dicyclohexylamine (DCHA) system: a novel and highly sensitive detection of DCHA via ECL-flow injection analysis. *Anal Chem.* 2021;93:6472–80.
- Xiao SY, Zhen SJ, Huang CZ, Li YF. Ultrasensitive ratiometric electrochemiluminescence for detecting AtxA miRNA using luminol-encapsulated liposome as effectively amplified signal labels. *Biosens Bioelectron.* 2021;186:113263.
- Zhang G, Chai H, Tian M, Zhu S, Qu L, Zhang X. Zirconium-metalloporphyrin frameworks-luminol competitive electrochemiluminescence for ratiometric detection of polynucleotide kinase activity. *Anal Chem.* 2020;92:7354–62.
- Zhu X, Liu H, Dai Y, Wang X, Luo C, Wei Q. Enhanced electrochemiluminescence of luminol based on Cu<sub>2</sub>O-au heterostructure enabled multiple-amplification strategy. *Biosens Bioelectron.* 2020;151.
- Bertoncello P, Forster RJ. Nanostructured materials for electrochemiluminescence (ECL)-based detection methods: recent advances and future perspectives. *Biosens Bioelectron.* 2009;24:3191–200.
- Zhu X, Zhang Y, Liu M, Liu Y. 2D titanium carbide MXenes as emerging optical biosensing platforms. *Biosens Bioelectron.* 2021;171:112730.
- Li Z, Zhuang T, Dong J, Wang L, Xia J, Wang H, Cui X, Wang Z. Sonochemical fabrication of inorganic nanoparticles for applications in catalysis. *Ultrason Sonochem.* 2021;71:105384.
- Sun J, Sun H, Liang Z. Nanomaterials in electrochemiluminescence sensors. *ChemElectroChem.* 2017;4:1651–62.
- Bertoncello P. Nanomaterials for biosensing with electrochemiluminescence (ECL) detection. *Frontiers in bioscience-landmark.* 2011;16:1064–108.
- Li Z, Dong J, Zhang H, Zhang Y, Wang H, Cui X, Wang Z. Sonochemical catalysis as a unique strategy for the fabrication of nano-/micro-structured inorganics. *Nanoscale Adv.* 2021;3:41–72.
- Khan MS, Zhu W, Ali A, Ahmad SM, Li X, Yang L, Wang Y, Wang H, Wei Q. Electrochemiluminescent immunosensor for prostate specific antigen based upon luminol functionalized platinum nanoparticles loaded on graphene. *Anal Biochem.* 2019;566:50–7.
- Wang S, Wang M, Li C, Li H, Ge C, Zhang X, Jin Y. A highly sensitive and stable electrochemiluminescence immunosensor for alpha-fetoprotein detection based on lumi-nol-AgNPs@co/Ni-MOF nanosheet microflowers. *Sens Actuators B Chem.* 2020;311:127919.
- Naguib M, Kurtoglu M, Presser V, Lu J, Niu J, Heon M, Hultman L, Gogotsi Y, Barsoum MW. Two-dimensional nanocrystals produced by exfoliation of Ti<sub>3</sub>AlC<sub>2</sub>. *Adv Mater.* 2011;23:4248–53.
- D, Chen C, Lu G, Song H. Ti<sub>3</sub>C<sub>2</sub> MXene quantum dots/TiO<sub>2</sub> inverse opal heterojunction electrode platform for superior photoelectrochemical biosensing. *Sens. Actuators B Chem.* 2019;289:131–137.
- Fatima U, Tahir MB, Sagir M, Fatima N, Nawaz T, Ashraf N. Two-dimensional materials and synthesis, energy storage, utilization, and conversion applications of two-dimensional MXene materials. *Int. J. Energy Res: Bhatti MP;* 2021.
- Liu Y, Yu J, Guo D, Li Z, Su Y. Ti<sub>3</sub>C<sub>2</sub>T<sub>x</sub> MXene/graphene nanocomposites: synthesis and application in electrochemical energy storage. *J Alloys Compd.* 2020;815.
- Riazi H, Nemani SK, Grady MC, Anasori B, So-roush M. Ti<sub>3</sub>C<sub>2</sub>MXene-polymer nanocomposites and their applications. *J Mater Chem A.* 2021;9:8051–98.
- Tang R, Xiong S, Gong D, Deng Y, Wang Y, Su L, Ding C, Yang L, Liao C. Ti<sub>3</sub>C<sub>2</sub> 2D MXene: recent progress and perspectives in photocatalysis. *ACS Appl Mater Interfaces.* 2020;12:56663–80.
- Zhang H, Wang Z, Zhang Q, Wang F, Liu Y. Ti<sub>3</sub>C<sub>2</sub> MXenes nanosheets catalyzed highly efficient electrogenerated chemiluminescence biosensor for the detection of exosomes. *Biosens Bioelectron.* 2019;124-125:184–90.
- Zhang H, Wang Z, Wang F, Zhang Y, Wang H, Liu Y. Ti<sub>3</sub>C<sub>2</sub> MXene mediated prussian blue in situ hybridization and electrochemical signal amplification for the detection of exosomes. *Talanta.* 2021;224:121879.
- Zhao D, Chen Z, Yang W, Liu S, Zhang X, Yu Y, Cheong WC, Zheng L, Ren F, Ying G, Cao X, Wang D, Peng Q, Wang G, Chen C. MXene (Ti<sub>3</sub>C<sub>2</sub>) vacancy confined single-atom catalyst for efficient functionalization of CO<sub>2</sub>. *J Am Chem Soc.* 2019;141:4086–93.
- Jiang Y, Zhang X, Pei L, Yue S, Ma L, Zhou L, Huang Z, He Y, Gao J. Silver nanoparticles modified two-dimensional transition metal carbides as nanocarriers to fabricate acetylcholinesterase-based electrochemical biosensor. *Chem Eng J.* 2018;339:547–56.
- Hui X, Zhao R, Zhang P, Li C, Wang C, Yin L. Low-temperature reduction strategy synthesized Si/Ti<sub>3</sub>C<sub>2</sub> MXene composite anodes for high-performance Li-ion batteries. *Adv Energy Mater.* 2019;9.
- Naguib M, Mochalin VN, Barsoum MW, Gogotsi Y. 25th anniversary article: MXenes: a new family of two-dimensional materials. *Adv Mater.* 2014;2:992–1005.
- Fang Y, Yang X, Chen T, Xu G, Liu M, Liu J, Xu Y. Two-dimensional titanium carbide (MXene)-based solid-state electrochemiluminescent sensor for label-free single-nucleotide mismatch discrimination in human urine. *Sens. Actuators B Chem.* 2018;263:400–7.
- Halim J, Kota S, Lukatskaya MR, Naguib M, Zhao MQ, Moon EJ, Pitock J, Nanda J, May SJ, Gogotsi Y, Barsoum MW. Synthesis



- and characterization of 2D molybdenum carbide (MXene). *Adv Funct Mater.* 2016;26:3118–27.
36. Nie Y, Yuan X, Zhang P, Chai YQ, Yuan R. Versatile and ultrasensitive electrochemiluminescence biosensor for biomarker detection based on nonenzymatic amplification and aptamer-triggered emitter release. *Anal Chem.* 2019;91:3452–8.
  37. Yao LY, Yang F, Liang WB, Hu GB, Yang Y, Huang W, Yuan R, Xiao DR. Ruthenium complex doped metal-organic nanoplate with high electrochemiluminescent intensity and stability for ultrasensitive assay of mucin 1. *Sens. Actuators B Chem.* 2019;292:105–10.
  38. Zhang H, Wang Z, Wang F, Zhang Y, Wang H, Liu Y. In situ formation of gold nanoparticles decorated Ti<sub>3</sub>C<sub>2</sub> MXenes nanoprobe for highly sensitive electrogenerated chemiluminescence detection of exosomes and their surface proteins. *Anal Chem.* 2020;92:5546–53.
  39. Shahsavari K, Shokri E, Hosseini M. A fluorescence readout method for miRNA-155 detection with double-hairpin molecular beacon based on quadruplex DNA structure. *Microchem J.* 2020;158:105277.
  40. Cai W, Xie S, Tang Y, Chai Y, Yuan R, Zhang J. A label-free electrochemical biosensor for microRNA detection based on catalytic hairpin assembly and in situ formation of molybdophosphate. *Talanta.* 2017;163:65–71.
  41. Zeng K, Li H, Peng Y. Gold nanoparticle enhanced surface plasmon resonance imaging of microRNA-155 using a functional nucleic acid-based amplification machine. *Microchim Acta.* 2017;184:2637–44.
  42. Wang F, Fu C, Huang C, Li N, Wang Y, Ge S, Yu J. Paper-based closed Au-bipolar electrode electrochemiluminescence sensing platform for the detection of miRNA-155. *Biosens. Bioelectron.* 2020; 150: 111917.
  43. Wang F, Liu Y, Fu C, Li N, Du M, Zhang L, Ge S, Yu J. Paper-based bipolar electrode electrochemiluminescence platform for detection of multiple miRNAs. *Anal Chem.* 2021;93:1702–8.
- Publisher's note** Springer Nature remains neutral with regard to jurisdictional claims in published maps and institutional affiliations.